Swinburne Research Bank
http://researchbank.swinburne.edu.au

Larsen, E. K. U., Nielsen, T., Wittenborn, T. et. al. (2012). Accumulation of magnetic iron oxide nanoparticles coated with variably sized polyethylene glycol in murine tumors.

Originally published in *Nanoscale, 4*(7) 2352-2361.
Available from: http://dx.doi.org/10.1039/c2nr11554a

Copyright © The Royal Society of Chemistry 2012.

This is the author's version of the work, posted here with the permission of the publisher for your personal use. No further distribution is permitted. You may also be able to access the published version from your library. The definitive version is available at http://pubs.rsc.org/ .

Accumulation of magnetic iron oxide nanoparticles coated with different sized polyethylene glycol in murine tumors

Esben Kjær Unmack Larsen[a], Thomas Nielsen[b], Thomas Wittenborn[b], Louise Munk Rydtoft[c], Arcot R. Lokanathan[a], Line Hansen[a], Leif Østergaard[b], Peter Kingshott[a,e], Ken Howard[a], Flemming Besenbacher[a] *, Niels Chr. Nielsen[d], Jørgen Kjems[a] *

[a] Interdisciplinary Nanoscience Center (iNANO), Departments of Molecular Biology, Physics and Astronomy, Aarhus University, DK-8000 Aarhus C, Denmark, [b] iNANO, Department of Experimental Clinical Oncology and Department of Neuroradiology, [c] iNANO, Danish National Research Foundations Center of Functionally Integrative Neuroscience Aarhus University Hospital, DK-8000 Aarhus C, Denmark, [d] Center for Insoluble Protein Structures (inSPIN), iNANO and Department of Chemistry, Aarhus University, DK-8000 Aarhus C, Denmark, [e] Current address: Faculty of Engineering and Industrial Sciences, Swinburne University of Technology, Hawthorn, Victoria 3122, Australia.

This work was supported by grants from The Danish Council for Strategic Research / Programme Commission on Nanoscience, Biotechnology, and IT (NABIIT), the Danish National Research Council, the Carlsberg Foundation, CIRRO - The Lundbeck Foundation Center for Interventional Research in Radiation Oncology and the Danish Cancer Society.

*Address correspondence to:

Flemming Besenbacher: fbe@inano.dk

Jørgen Kjems: kjems@inano.dk

Keywords:

Magnetic resonance imaging; cancer; magnetite nanoparticles; ultra small superparamagnetic iron oxide (USPIO) particles; polyethylene glycol; molecular weight; nanomedicine; tumor imaging; coating

TOC figure

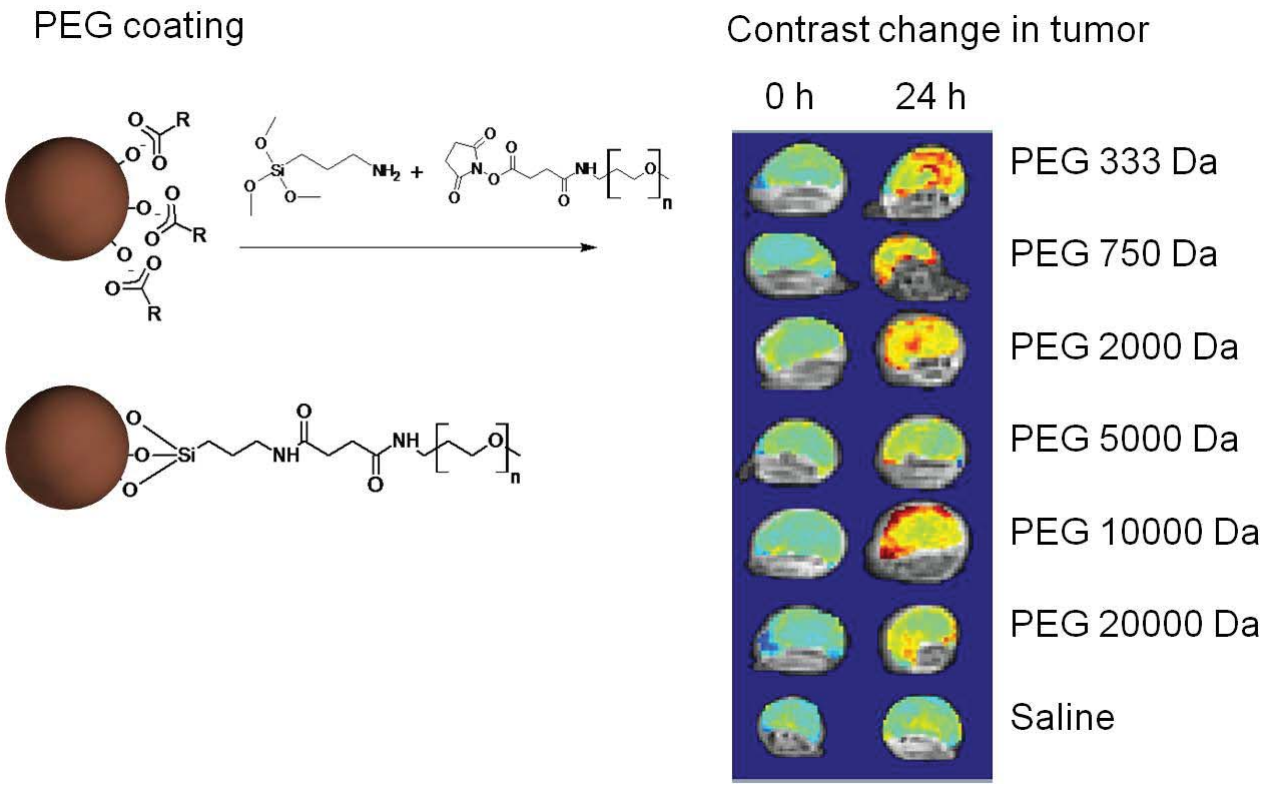

Abstract

Iron oxide nanoparticles have found widespread applications in different areas including cell separation, drug delivery, and as contrast agents. Due to water insolubility and stability issues, nanoparticles utilized for biological applications require coatings such as the commonly employed polyethylene glycol (PEG). Despite its frequent use, the influence of PEG coatings on the physicochemical and biological properties of iron nanoparticles has hitherto not been studied in detail. To address this, we studied the effect of 333-20000 Da PEG coatings that resulted in larger hydrodynamic size, lower surface charge, longer circulation half-life, and lower uptake in macrophages cells when the particles were coated with high molecular weight (Mw) PEG molecules. By use of magnetic resonance imaging, we show coating-dependent in vivo uptake in murine tumors with an optimal coating Mw of 10000 Da.

Introduction

Magnetic nanoparticles (MNP) have gained much attention as contrast-enhancing agents for magnetic resonance imaging (MRI), as the sensitivity is significantly increased by MNP accumulation [1]. The most

commonly used MNPs are composed of an iron oxide core consisting of crystal magnetite (Fe_3O_4) or maghemite (γFe_2O_3). Increased contrast in areas containing the MNPs is due to disturbance of the MRI signal by the magnetic properties of the iron oxide core [2].

Surface coating that include dextran, citrate, or polyethylene glycol (PEG), provide stability and enhanced biocompatibility to the MNPs[3]. PEG is a common polymer used for coatings and is composed of a biocompatible polyether with a repeat unit of CH_2-CH_2-O- that can be of different chain lengths [4-7]. PEG is hydrated in water due to the oxygen atoms within the ether group interacting with approximately two water molecules [8]. This increases the molecules' water solubility and decreases toxicity and immunogenicity [9]. Due to the simple structure and chemical stability of PEG is often used as an biocompatible polymer. Moreover, this polymer and many derivatives have been FDA approved and used clinically as carriers in pharmaceutical formulations [10]. Drugs or nanoparticles coated with PEG typically have reduced interactions with the mononuclear phagocyte system (MPS), and the complement system resulting in an increased circulatory half-life [10-15].

The size of nanoparticles can influence their biodistribution. Large nanoparticles with a hydrodynamic diameter from 65 to 200 nm have been reported to accumulate primarily in the liver and spleen but also in other organs including the bone marrow, heart, kidneys, stomach, and lungs [16-19]. Smaller particles below 20 nm have been reported to be removed from the blood by renal excretion in the kidneys [20;21]. The PEG layer can increase the hydrodynamic diameter of particles [6;7;22;23]. Gref *et al.* reported that PLGA nanoparticles coated with PEG had a higher circulation half-life and decreased liver accumulation with increasing molecular weight (Mw) of PEG suggesting a reduction in MPS uptake [24]. Another study confirmed that macrophages have a lower uptake of nanoparticles coated with high Mw PEG compared to low Mw PEG [25]. This could be a consequence of reduced interaction between the protein opsonins in blood and nanoparticles coated with high Mw PEG (>5000 Da) compared to particles with low Mw PEG of 2000 Da [15].

It is generally believed that increased angiogenesis in tumors, resulting in an abnormal micro-vasculature, with leaky endothelium and inadequate formation of the lymphatic system can create a phenomenon known as the Enhanced Permeability and Retention (EPR) effect [26;27]. Nanoparticles small enough to penetrate the leaky vessels have previously been used as tracers for MRI to visualize tumors

and we previously reported that MNPs with a larger iron oxide core increased the contrast in tumors after injection of the nanoparticles [3;11;28;29].

Most knowledge concerning the effect of nanoparticle coating on cellular uptake, circulatory blood half-life, and the ability to accumulate in tumors derives from investigations with non-magnetic nanoparticles whereas information concerning MNP coatings is still rare. In this study, we address synthesis and coating of iron oxide nanoparticles with variably sized PEG (Mw between 333-20000 Da) and investigate the effect on the physicochemical and biological properties. We show Mw-dependent in vivo uptake in mice tumors, with an optimal PEG length of 10000 Da.

Materials and methods

Materials

Oleic acid, pentane, toluene, iron(III) chloride pentahydrate, ($FeCl_3$ - $5H_2O$), iron(II) chloride tetrahydrate ($FeCl_2$ - $4H_2O$), triethylamine (TEA) were purchased from Sigma-Aldrich. RPMI media from Invitrogene. FerroZine Iron Reagent Solution was acquired from HACH, TEM grid, kohle lochfilme acquired from Plano. 2,5,8,11-Tetraoxatetradecan-14-oic acid succinimidyl ester (NHS-PEG: 333 Da) from IRIS biotech GmbH. Methoxy PEG Succinimidyl active esters (NHS-PEG: 750, 2000, 5000, 10000, 20000 Da) were purchased from Rapp-polymere GmbH. 100K Nanosep Spin Filters were acquired from VWR.

Synthesis of oleic acid coated iron oxide magnetic nanoparticles (MNP)

In a typical experiment, 1.08 g $FeCl_3$ - $5H_2O$ and 0.40 g $FeCl_2$ - $4H_2O$ were dissolved in 20 ml water. In a 3-neck bottle 20 ml NaOH (1M), 10 ml acetone, and 0.2 ml oleic acid were added and the solution was heated to 83 $^{\circ}$C. For 5 min nitrogen gas was flowed through both solutions, and a continuous flow of nitrogen through the reaction was established throughout the whole experiment. During rapid stirring (1200 rpm), the iron solution was added drop-wise to the solution over a period of 5 min. Thereafter, 0.8 ml oleic acid was added to the solution over a period of 10 min. After 10 min, the solutions were precipitated with methanol/ethanol (1:1), collected with a neodymium magnet and supernatant was discarded. This washing process was repeated three times.

Synthesis of silane coated MNPs

Twenty milligrams of MNPs coated with oleic acid were dissolved in toluene in a glass tube at a concentration of 5 mg/ml. To this solution, were sequentially added Si-NH_2, TEA and H_2O during stirring together with NHS-PEG. To coat oleic-acid-coated MNPs with NHS-PEG, the optimal coating procedure required 6 µl Si-NH_2 with a NHS-PEG/Si-NH_2 ratio of 1.5 (17 mg NHS- PEG 333 Da, 38 mg NHS-PEG 750 Da, 100 mg NHS-PEG 2000 Da, 251 mg NHS-PEG 5000 Da, 502 mg NHS-PEG 10000 Da, 1004 mg NHS-PEG 20000 Da. After 24 hours, the particles were precipitated with pentane and the supernatant was discarded. Subsequently, the particles were re-dissolved in toluene and precipitated with pentane. After repeating the washing procedure three times, the nanoparticles were dissolved in water and centrifuged for 2 minutes at 10k rpm to remove any aggregates.

Cellular uptake studies

RAW 264.7 and J774A.1 cells were grown in the RPMI media with 10% fetal bovine serum and 1% penicillin/streptomycin. In a typical experiment, MNPs were added to cell suspensions in 24 well plates to a final iron concentration of 0.05 mg/ml and incubated for 24 hours. The cells were then washed three times with PBS and lysed with 50 µl of lysis buffer for 24 hours. The protein content was measured by UV/Vis spectrophotometry (). 25 µl of the lysate was added to 200 µl Bradford's reagent and the absorbance measured at 595 nm. The protein concentration in the lysates was determined against a standard curve of absorbance vs concentration of BSA. The iron concentration was determined by adding 25 µl HCl (12M) to 25 µl lysate solution followed by 2 hours of incubation to dissolve the nanoparticles. Two hundred microlitres of H_2O mixed with 50 µl ferrozin solution was added to the solution and the absorbance was measured at 562 nm. The iron concentration and was determined using a standard curve of absorbance vs $FeCl_3$ concentration..

MRI studies

SCCVII squamous cell carcinomas were implanted into the right rear foot of C3H mice, and C3H mammary carcinomas were implanted into the right rear foot of CDF_1 mice. Experiments were performed when the tumor sizes reached approximately 200 mm^3. The tumour volume was calculated from the formula $D1 \times D2 \times D3 \times \pi/6$, where D1, D2, and D3 represent the three orthogonal diameters. All experiments were performed under national and European Union-approved guidelines for animal welfare.

MRI was performed before and 24 hours following intravenous injection with MNPs using either a 3 T system (Signa Excite HD, General Electric Medical Systems, Milwaukee, WI) or a 16.4 T system (Bruker Avance II widebore NMR spectrometer, Bruker BioSpin GmbH, Rheinstetten, Germany) equipped with a Micro 2.5 imaging probe. For 3 T MRI, mice bearing SCCVII squamous cell carcinomas or C3H mammary carcinomas were restrained in specially constructed lucite jigs with the tumor-bearing leg exposed and loosely attached to the jig with tape without impairing the blood supply to the foot. Two mice were positioned in an upper extremity quadrature radiofrequency coil (Mayo Clinic BC-10 3.0 T, General Electric Medical Systems, Milwaukee, WI), and their tumours were scanned simultaneously. The imaging protocol included a spin echo sequence with different echo times (T_E) for R_2 estimation. A single slice of 2 mm thickness was placed through the tumor centers. The imaging parameters were: T_R = 2 s, field of view = 4×4 cm, acquisition matrix 128×128, number of averages = 1, the eight T_E values acquired in two excitation were 15; 30; 40; 45; 60; 80; 120; 160 ms.

For 16.4 T MRI, mice bearing C3H mammary carcinomas were anesthetized with 10 µl/g Ketamine/Xylazin mixture (10 mg/ml Ketamine + 1 mg/ml Xylazin), and the tumor-bearing foot was restrained in a coil measuring 25 mm in inner diameter. An intraperitoneal line was inserted for administration of top-up anesthesia. The imaging protocol included a spin echo sequence with 16 different T_E acquired in one excitation for R_2 estimation. 26 slices of 0.2 mm thickness were planned. The imaging parameters were: T_R approximately 4 s, field of view = 2×2 cm, acquisition matrix 256×192, number of averages = 1, shortest T_E value approximately 10 ms.

The relaxation of the iron oxide nanoparticles was estimated by measuring the relaxation rate R_2 of iron oxide in different concentrations (0, 0.56, 3.33, and 20 µg [Fe]/ml). The different formulations were contained in individual 5 mm NMR tubes, which were put in a glass with water to minimize susceptibility artifacts, and MRI was performed at 3 T. 5 slices of 2 mm thickness was placed such that cross sections of all tubes were visible. The imaging parameters were: T_R = 2 s, field of view = 6.5×6.5 cm, acquisition matrix 128×128, number of averages = 1, the eight T_E values acquired in two excitation were 15; 30; 40; 45; 50; 100; 150; 200 ms. Data analysis was performed using MATLAB 7.11 (The MathWorks, Inc., Natick, MA, USA). R_2 maps were produced using nonlinear least squares fitting of the image signal S to the equation $S(TE) = S(0)*\exp(-T_E*R_2)$. The relaxivity of the nanoparticles was calculated as the slope in a plot of R_2 vs. iron concentration ($r > 098$ for all samples).

Circulatory half-life

Blood samples were taken from C3H mice before and 5 min, 1 hour, 6 hour, and 24 hour after injection of nanoparticles (5 mg [Fe]/kg mice). Three mice were used for each nanoparticle formulation. EDTA plasma was collected after centrifugation of the blood samples. The plasma was digested with 5.5 ml HNO_3 (69% v/v) and 0.5 ml HCl (37% v/v) in a microwave oven (Milestone Ethos 1600). The iron concentration was analyzed using an inductively coupled plasma atomic emission spectroscopy (ICP-AES (Plasma 2000, Perkin-Elmer, USA). The half-life was calculated based on the injected concentrations and the measurements of iron concentration in the blood after 5 min and 1 hour. The half-life was determined by regression analysis, calculated based on an exponential decay.

Iron oxide concentration

To measure the concentration of MNPs, 10 µl sample were dissolved in 10 µl of HCl. The samples were then diluted to 300 µl and 10 µl was added to a 200 µl H_2O with 50µl ferrozin solution and absorbance measured at 562 nm. This was correlated to a standard curve to give the iron concentration.

FTIR, TEM, DLS, and XPS measurements

For FTIR spectroscopy, the samples were air-dried, mixed with potassium bromide and pressed to a pellet. Subsequently, they were analyzed using a Fourier transform spectroscopy (FTIR) on a Perkin-Elmer Paragon 1000 FTIR spectrometer.

Transmission electron microscopy (TEM) was performed on samples air-dried on 300 mesh copper grids and visualized using a 200 kV Philips CM20 microscope. For each MNP formulation, the mean size value was calculated ± standard deviation based on more than 50 particles.

The hydrodynamic size and zeta potential of the nanoparticles were determined using Dynamic light scattering (DLS) using a Zetasizer Nano ZS (Malvern Instruments, Malvern, UK). All measurement was made in phosphate buffered solution at pH 7.

XPS spectra were recorded using a Kratos Axis Ultra^{DLD}machine operating with a power of 150 W (15 kV and 10 mA). The samples was mounted on Al stubs, and dried out over night. The spectra were recorded using monochromated $Al_{k\alpha}$ x-rays (1486 eV) from an with pass energies of 20 and 160 eV for high-resolution and survey spectra, respectively. A hybrid lens mode was employed during analysis (electrostatic and magnetic). The XPS spectra for all samples were taken at a photoemission angle of 0°,

and the analysis area was 700-300 μm. The Kratos charge neutralizer system was used on all samples with a filament current between 1.8 and 2.1 A and a charge balance of 3.6 V. The measured binding energy positions were charge corrected with reference to 285.0 eV, corresponding to the C-C/C-H species. The generated data were converted into VAMAS format and analyzed using CasaXPS software.

Statistics

All graphs show mean value and standard deviation. Statistical significance was calculated using two tailed student t-test assuming equal variance.

Results

Physicochemical properties of nanoparticles coated with different Mw PEG

Functionalized MNPs was made using a strategy previously reported [3] (Figure 1).

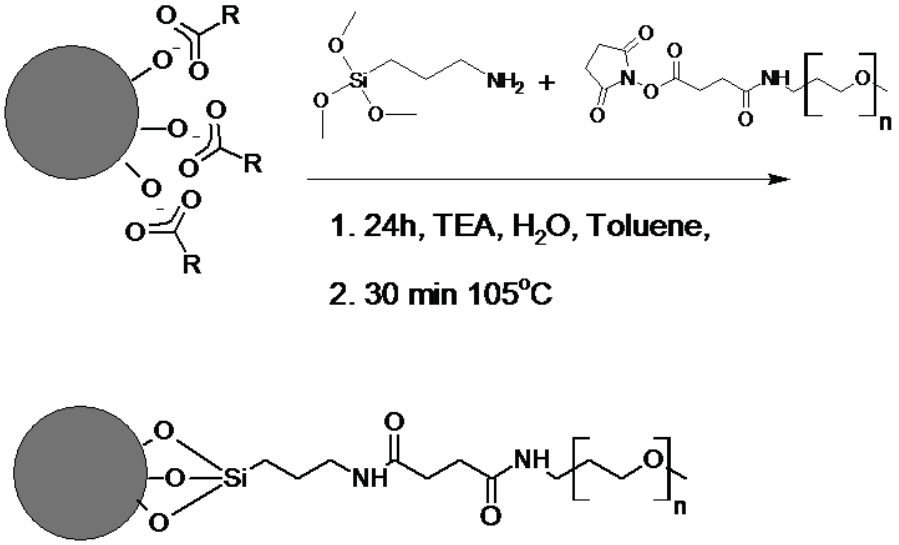

Figure 1 Reaction scheme of coating oleic acid nanoparticles with silane conjugated to PEG.

The conditions for MNP coating were optimized using 2000 Da NHS-PEG (supplementary information) and used for preparation of MNPs with Si-NH_2 and NHS-PEG of different Mw (333, 750, 2000, 5000, 10000, and 20000 Da).

Application of Fourier transform infrared spectroscopy (FTIR) spectra of PEG-coated particles showed a clear difference between nanoparticles coated with PEG (Figure 2 a-f) and the precursor particles coated with oleic acid (Figure 2 g). The spectra of oleic acid coated particles revealed only a few identifiable bands including the Fe-O vibration band at 577 cm^{-1} and FeO-H vibration at 3400 cm^{-1}. The band at 1405 cm^{-1} could be assigned to the C-H bending vibrations primarily from the oleic acid chain. The band

from the iron oxide could also be identified on all the PEG coated particles. Conversely, the band from the C-H bending vibration at 1405 cm^{-1} were less distinct on the PEG coated particles.

The pure Si-NH_2 spectra had an amine N-H bending band around 1600 cm^{-1} (Figure 2 h). After conjugation of the Si-NH_2 with NHS-PEG, the amine was converted into an amide group and the N-H bending band was shifted to around 1650 cm^{-1}. This amide band was identifiable on all the spectra of the PEG coated particles.

The spectra of pure NHS-PEG (750 and 10000 Da) and the PEG coated particles have many identical peaks (Figure 2 i-j). The peaks at 800 and 950 cm^{-1} can be assigned to C-H rocking in the PEG chain, the peak at 1100 cm^{-1} most likely derives from the C-O stretch in the ether groups, and the band around 2900 cm^{-1} can be assigned to C-H stretch in the PEG chain. For coated particles, it is interesting to note that these four bands all grow in amplitude as the Mw of the PEG is increased, which is probably due to an increased amount of PEG relative to the iron oxide core. Overall, FTIR of the PEG coated particles confirmed that the particles were successfully coated with PEG.

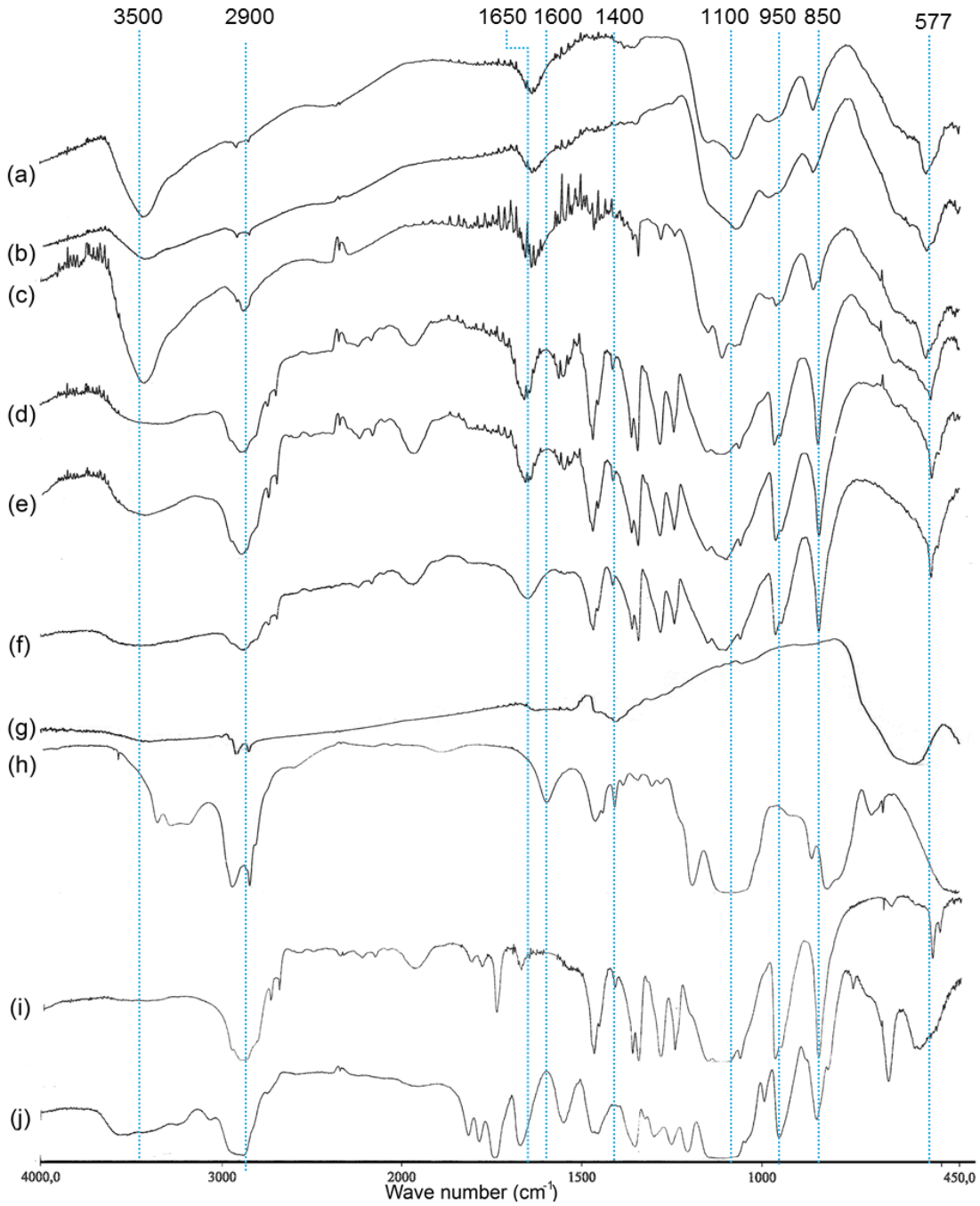

Figure 2 FTIR spectra of MNP with different PEG coatings. (a-f) Iron oxide nanoparticles coated with PEG of different Mw [(a) 333, (b) 750, (c) 2000, (d) 5000, (e) 10000, and (f) 20000 Da], (g) Oleic acid coated iron oxide nanoparticles, (h) Si-NH_2, (i) Pure 750 Da PEG, and (j) Pure 10000 Da PEG.

Transmission electron microscopy (TEM) images of the particles showed that the iron oxide cores appeared very similar with sizes of 8-10 ± 2nm independent of chemical coating (Figure 3a,b). It is not possible to visualize the PEG coating using this method, because of their low electron density.

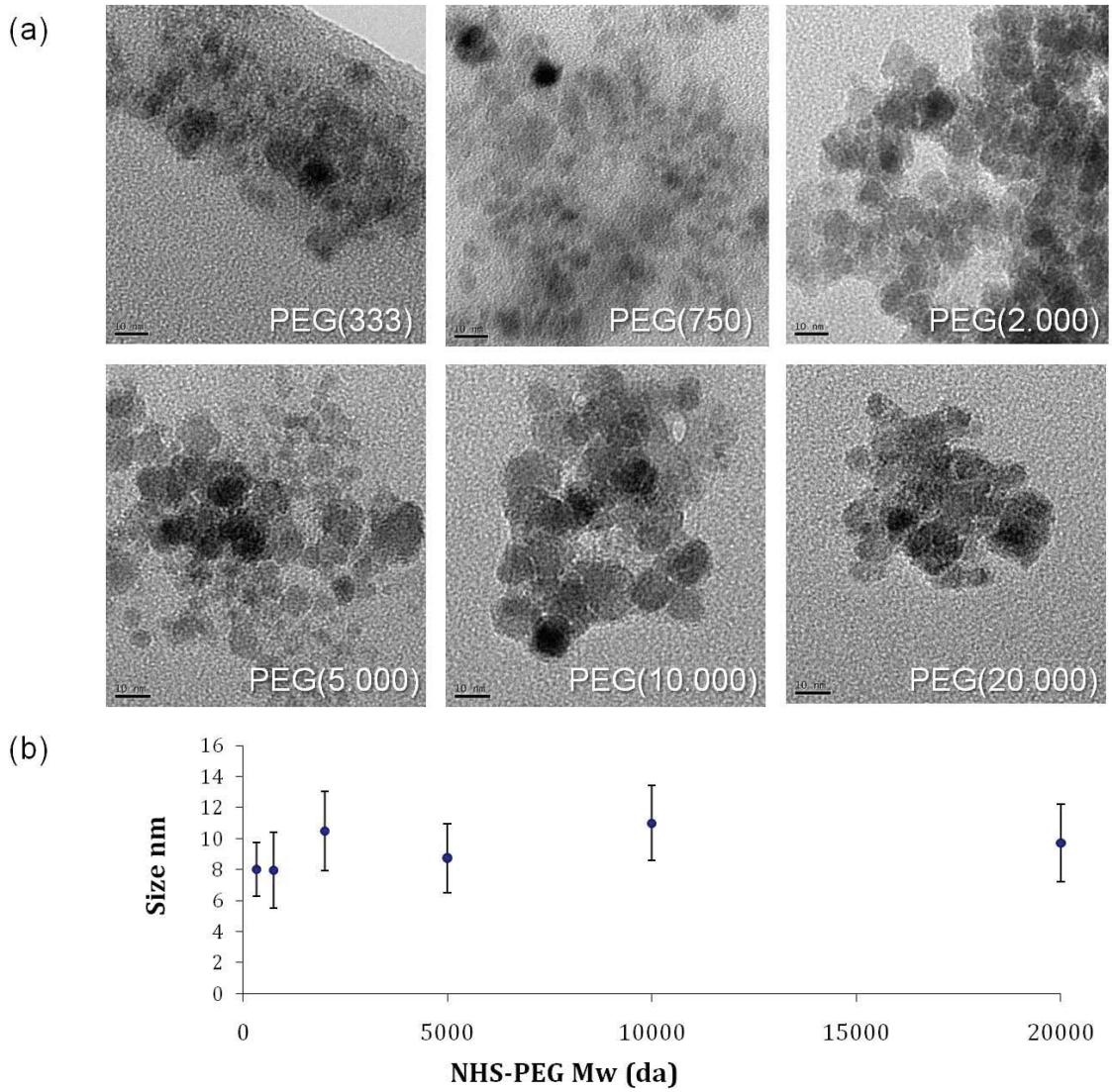

Figure 3 TEM images of MNP with different PEG coatings. (a) TEM images of iron oxide nanoparticles coated with PEG (scale bar 10nm). (b) Average size as a function of PEG Mw, based on measuring the diameter of 100 nanoparticles.

The hydrodynamic size of the particles, which includes the hydrodynamic water layer, was measured with dynamic light scattering (DLS) (Figure 4 a). This revealed an expected characteristic increase in particle size when increasing Mw of the PEG. The particles coated with the short PEG molecules of 333

and 750 Da both had a hydrodynamic size of approximately 20 nm, whereas MNPs with 2000-10000 Da PEG molecules measured 52-55 nm. MNP with 20000 Da PEG had the largest size with an average diameter of 67 nm.

The zeta potential increased with increasing Mw of the PEG: from -15.2 mV for the 333 Da particles to -2.6 mV for the particles coated with the longest PEG of 20000 Da (Figure 4).

The DLS size and zeta potential measurements clearly showed that the PEG coating influences the physical properties of the particles, and their similar response, upon increasing the PEG size, suggests that the hydrodynamic size and the shielding of the negatively charged core of the particle are closely linked.

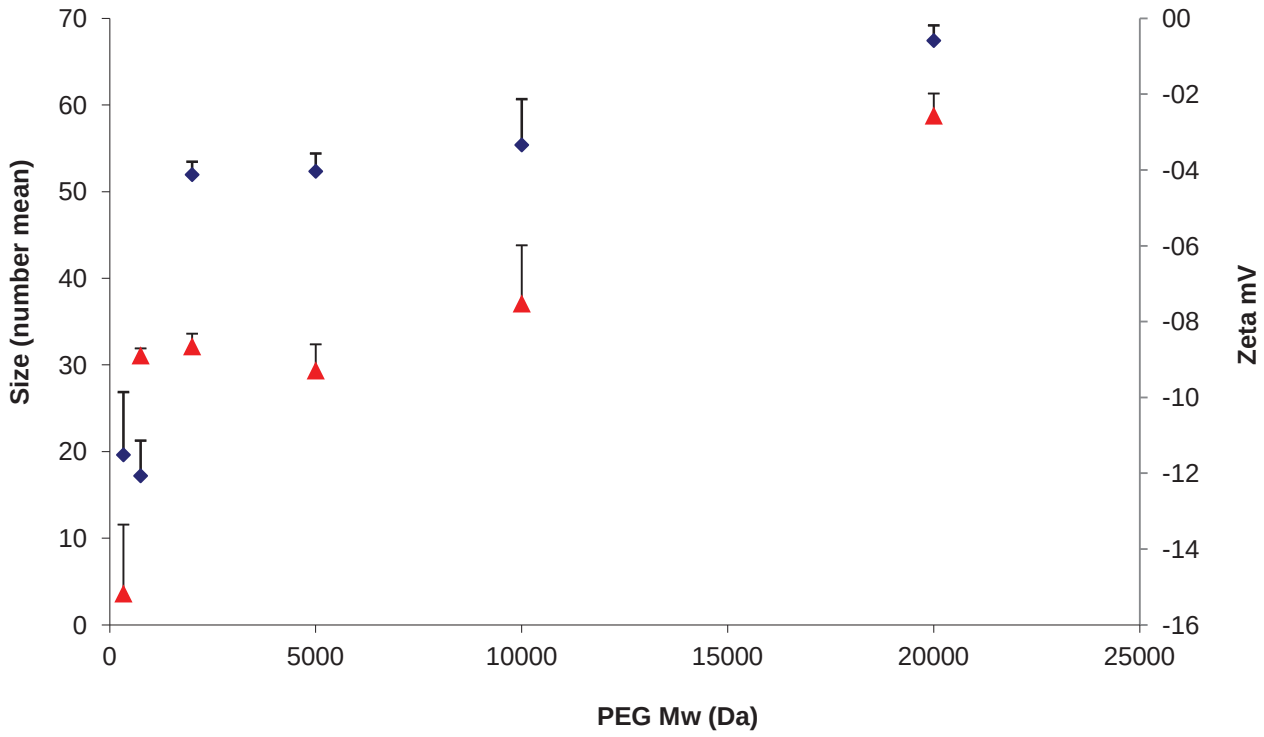

Figure 4 Size and zeta potential measurements for MNP with different Mw PEG molecules. Nanoparticles mean size (blue squares ◆) and zeta potential (red triangle ▼) measured with DLS.

X-ray photoelectron spectroscopy (XPS) studies of the coated nanoparticles provided qualitative and quantitative information about their surfaces chemistries. The survey spectra quantitatively indicated the

presence of various elements corresponding to the composition of particles. In the high resolution C 1s spectra, a contribution from oleic acid was found on the particles coated with the low Mw PEG (see supplementary information). The ratios of relative atomic percentages of carbon and iron obtained from the survey spectra of particles functionalized with PEG of different Mw indicated a correlation between C/Fe ratio and molecular weight of PEG (Figure 5a). A general increase in the thickness was observed with increasing Mw of PEG, from a thickness of 3.5 nm for the 333 Da coated particles to 6.5 nm for the 20000 Da PEG coated particles (Figure 5b). The thickness of the layer was determined using equation 1, based on attenuation of Fe 2p peak intensity [30;31]. The quantitative effect of nanoparticle curvature on the signal was taken into consideration by assuming the value of θ to be 57.3°, as proposed by Frydman et al. [32]. Information about calculating the inelastic mean free path of Fe 2p photoelectrons is included in supplementary information [33].

$$\frac{I}{I_o} = \exp\left(-\frac{L}{\lambda \cos\theta}\right) \quad \text{Eqn 1}$$

Equation 1. Attenuation of Fe 2p peak intensities. I_0 and I are intensities before and after PEG functionalization, respectively, L is the thickness of PEG layer, λ is the inelastic mean free path of Fe 2p photoelectron in carbon film, which is 1.5 nm [31], and θ is the take-off angle of 57.3°, which is the average angle of emission for a randomly rough particle surface.

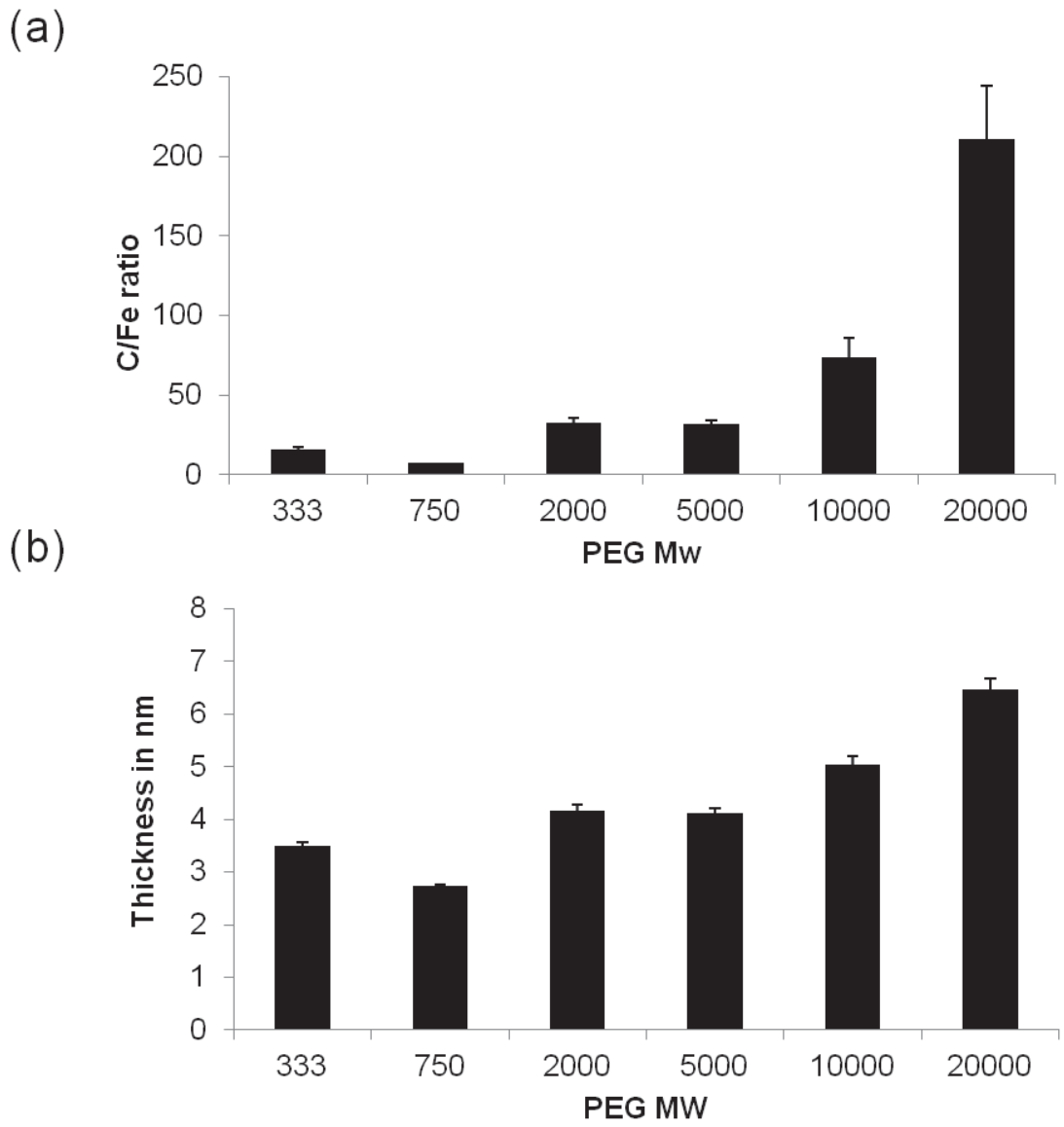

Figure 5 XPS analysis of MNP with different Mw PEG coatings. (a) Comparison of ratio of relative atomic percentage of carbon (C 1s) to iron (Fe 2p). (b) Comparison of overlayer thicknesses of nanoparticles after PEG coatings.

The relaxivity values were obtained on a 3 T MRI scanner and calculated for the iron oxide nanoparticles by measuring the relaxation rate at three different concentrations (20, 3.33, and 0.56 μg [Fe]/ml) using water as the background value. Calculation of the r_2 relaxivity revealed a clear influence from the PEG coating (Figure 6). The particles coated with the short 333 Da PEG had a low r_2 value of 97 $mM^{-1}s^{-1}$ whereas the particles coated with 5000 Da PEG had the highest r_2 value of 354 $mM^{-1}s^{-1}$. The trend was that the particles coated with Mw > 5000 Da PEG had declining r_2 compared to the 5000 Da PEG particles.

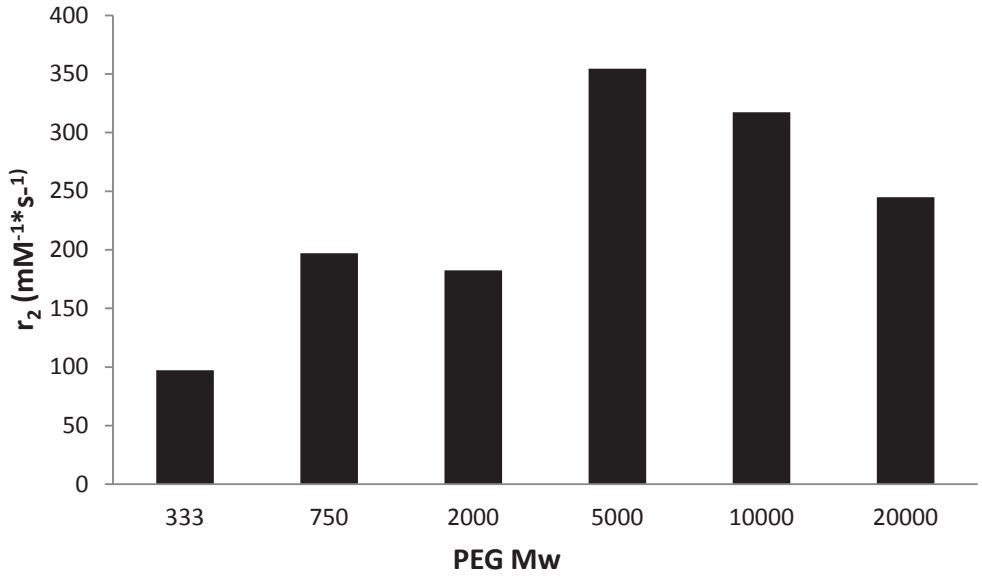

Figure 6 Relaxivity of MNP coated with different molecular weight PEG.

Cellular accumulation in vitro and in vivo studies

We examined the influence of the PEG chain length on macrophage uptake. Addition of particles to the J774A.1 macrophages cell-line revealed a larger uptake of the particles coated with low Mw PEG compared to the particles coated with high Mw PEG (Figure 7). The uptake for MNPs coated with 333 Da PEG was 0.0118 ± 0.0014 μg iron/μg protein which was significantly higher (P=0.0015) than the uptake of 0.0034 ± 0.0006 μg iron/μg protein for nanoparticles coated with 20000 Da PEG.

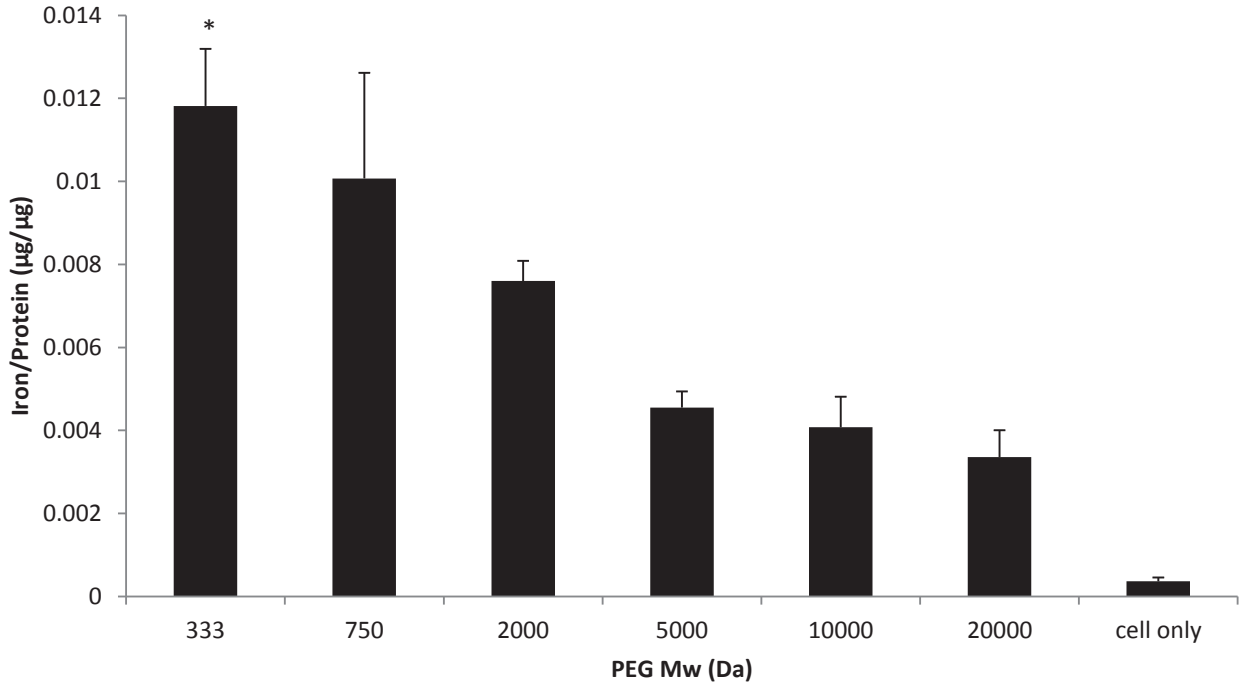

Figure 7 Uptake of nanoparticles in J774A.1 macrophage cell line coated with different Mw PEG. n=3, mean value + standard deviation.

The blood circulation time of the nanoparticles in mice was measured by determining the iron content in plasma from blood samples taken 5, 60, and 360 min after injection. Three MNP formulations (750, 2000, and 20000 Da PEG) were analyzed. Particle half-life increased with increasing Mw of the PEG from 20 min for 750 Da PEG to 45 min for 20000 Da PEG coated particles (Figure 8).

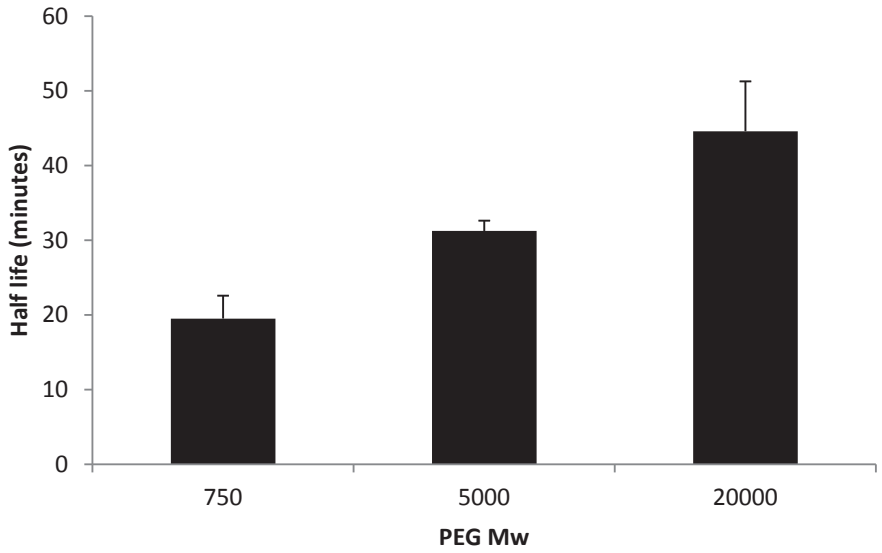

Figure 8 Blood circulation half-life of MNP coated with different molecular weight PEG. n=3, mean value + standard deviation.

The distribution of particles was examined in mice grafted with a subcutaneous squamous cell carcinoma (SCCVII) on the right foot of the hind leg (n=3) using a 3 T MR scanner. MRI images were recorded before and 24 hours after injection of nanoparticles (2.5 mg Fe/kg mice). An increase in relaxation rate R_2 was detected in the tumors for all particles with the smaller particles being more evenly spread over the tumor volume. In contrast, the larger particles seems to accumulate more intensely at the outer rim of the tumor (Figure 9a). A region of interest (ROI) was drawn around the tumor and a mean R_2 value was calculated for each tumor. The increase of contrast 24 hours after injection was largest for particles coated with 10000 Da PEG with an increase in R_2 of 60 % ± 12.5 % ($p = 0.0037$ compared to mice injected with saline; Figure 9 b). Compared to the other nanoparticles the accumulation of PEG 10000 is statistically different from both PEG 333 ($P=0.014$) and PEG 5000 ($P=0.011$). However, for particles coated with PEG 750, 2000 and 20000 it was not possible to statistically show any difference between PEG 10000 and these particles. The other particles all yielded lower R_2 values within the variability of the assay, where particles coated with 2000 Da PEG had a local maximum.

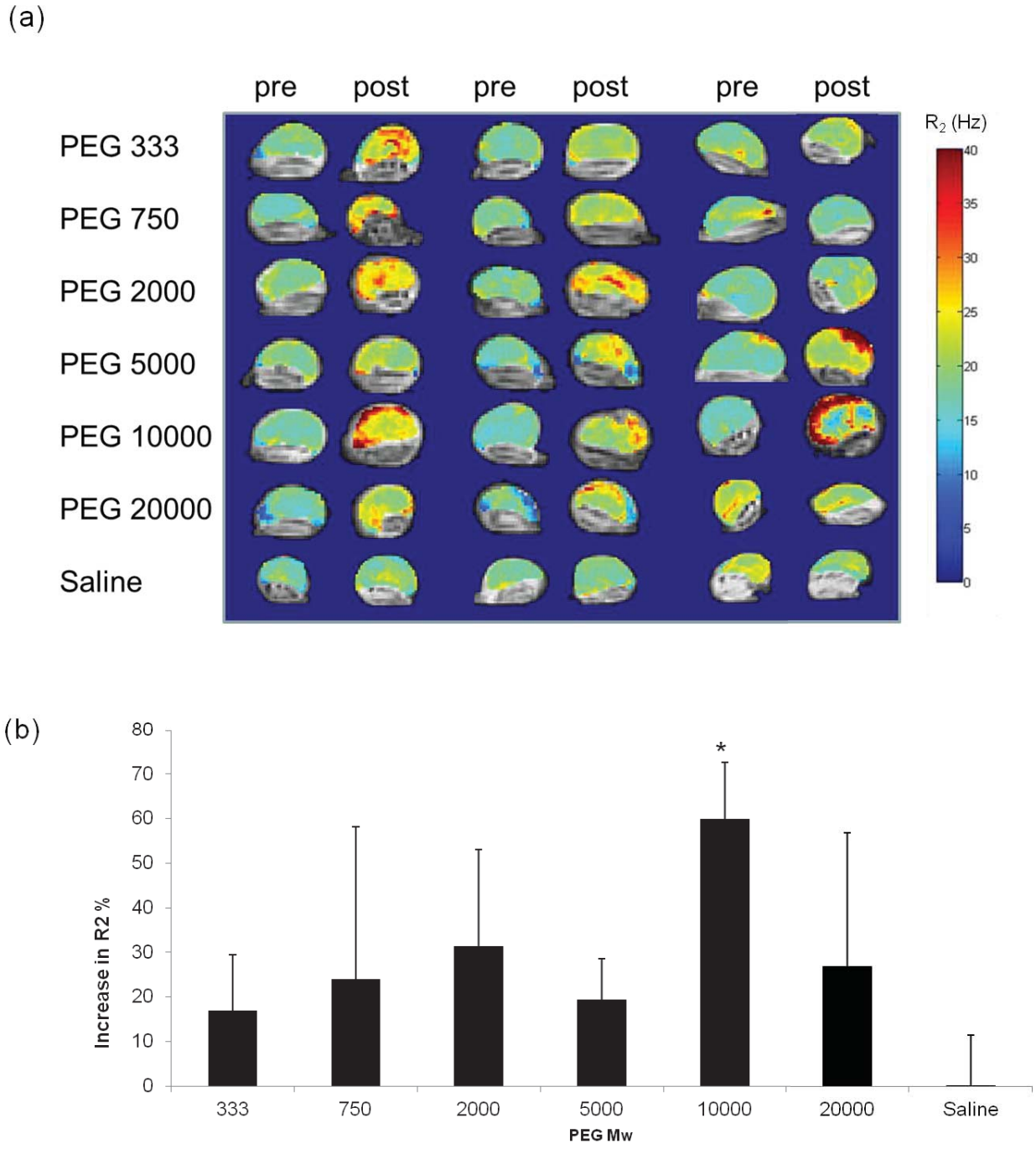

Figure 9 MRI of the foot on the hind leg of mice with a subcutaneous SCCVII tumor implanted using the 3 T scanner. (a) Images of the tumor before (pre) and after (post) injection of MNPs with different molecular weight PEG. Color-coded R_2 ROI on a T_2 weighted images. (b) Increase of the contrast mean R_2 value in a region of interest drawn around the tumor. n=3, mean value + standard deviation, * p = 0.0037 compared to mice injected with saline.

To compare tumor accumulation in a different model, each MNP with a different Mw PEG was injected into three animals implanted with C3H mammary carcinomas in the right hind foot. In this case the 3 T MRI images showed no difference in the accumulation of the particles (data not shown). With the aim of providing more detailed information, the experiment was repeated for the latter model using a high-field MRI 16.4 T scanner. At this ultra-high magnetic field strength, it is possible to obtain substantially higher resolution images of the tumor (Figure 10). Post injection of the nanoparticles, a change in contrast was seen with larger dark spots corresponding to lowered T_2 values in the tumor (i.e., increased relaxation rate). As the nanoparticle is a negative contrast agent, this can be interpreted as regional accumulation of nanoparticles. Especially after injection of nanoparticles coated with 750, 2000, and 10000 Da PEG, there were larger areas with very low signal intensity which match reasonably well with the two maxima observed for the other tumor model. These effects were not, however, quantified in more detail because the large susceptibility effect from the NPs at this high field strength resulted in a loss of signal already at the lowest echo time possible.

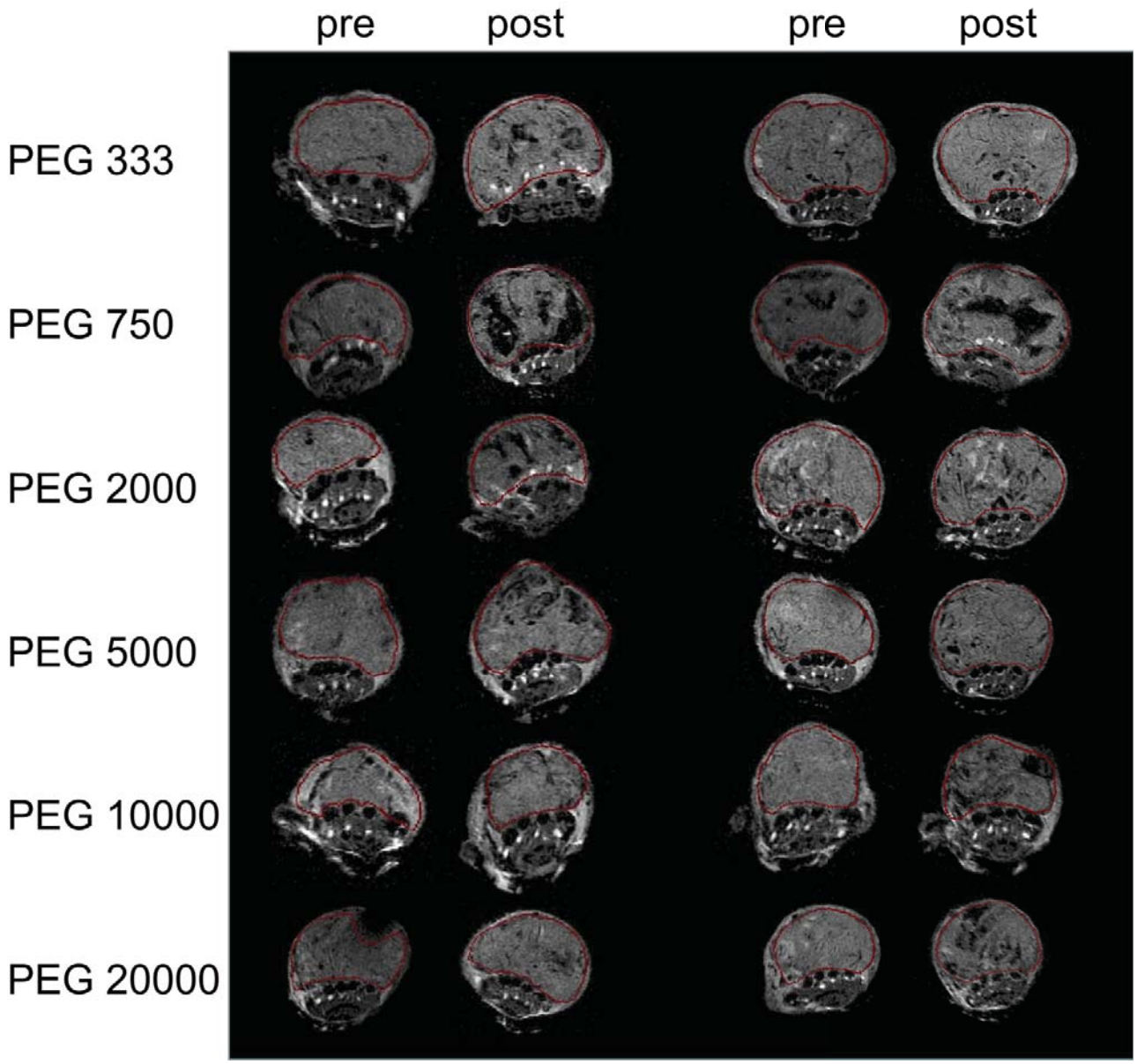

Figure 10 High-field (16.4 T) MRI of the foot on the hind leg of mice with a subcutaneous C3H tumor implanted marked by red line before (pre) and after (post) injection of MNPs with different molecular weight PEG.

Discussion

The general difficulties to obtain sufficient contrast in a tumor with MNPs motivated us to optimize parameters that influence nanoparticle stability, macrophage uptake and biodistribution in tumor bearing mice. High stability of nanoparticles is of key importance for *in vivo* application, as unstable particles have been shown to exhibit higher toxicity. The reduction in phagocytic capture is a requirement for prolonged circulation and a prerequisite for subsequent accumulation in tumors. Furthermore, aggregation of MNPs greatly limits the possibility of the nanoparticles reaching the tumor [34].

TEM studies revealed a similar core size of 8-10 ± 2 nm independent of the chemical treatment (Figure 2) and FTIR analysis confirmed successful surface PEGylation to a reactive silane group on the MNPs (Figure 3) The hydrodynamic sizes of the particles increased with increasing Mw of the PEG presumably due to the longer PEG chain and increased hydration (Figure 4) [7]. XPS analysis revealed that the relative amount of carbon (i.e. from PEG) to iron increased with higher Mw of PEG, indicating more extensive PEG coating when using high Mw PEG. The thickness was calculated from the decrease in Fe signal, and was found to increase from with higher Mw PEG. With a similar trend the zeta potential of the particles increased towards zero with longer PEG chains, which may be explained by increased shielding of the negative charge of the core. This could contribute to the reduction in phagocytosis of the larger particles in our study (Figure 7) and be supported by previous studies showing a reduced uptake of neutral particles in phagocytic cells compared to charged nanoparticles [35;36].

The PEG layer changed the relaxivity of the particles, resulting in an increased r_2 value with increasing Mw of the PEG until a plateau is reached at 5000 Da (Figure 6). Previous studies have also shown that the relaxivity is dependent on the coating, albeit with conflicting results [7;37;38]. Laconte et al. synthesized particles coated with PEG and showed that the r_2 value decreased with increased Mw of the PEG [7]. In contrast, Rowe et al made gadolinium nanoparticles coated with PHPMA or PNIPAM of three different length polymer (Mw ~5000, ~10000, and ~20000 Da) and observed increased r_2 values when increasing the length of the polymer [37]. Duan *et al.* examined the influence of the coating on the r_2 value and found that a more hydrophilic coating resulted in a larger r_2 value. As the particles in this study were coated with hydrophilic PEG molecules, this could explain the large r_2 value of particles coated with 5000 Da PEG chain, but is inconsistent with the declined r_2 value for 10000 and 20000 Da PEG. From the XPS analysis of the nanoparticles, it is clear that there is some remaining oleic acid on the particles coated with the low Mw PEG. This oleic acid could prevent water from reaching the core of the nanoparticles, resulting in a low relaxivity for these particles. It should also be noted that when MNPs are taken up in cells, the relaxivity can change, because the iron oxide core from several nanoparticles is condensed into one particle [39-41]. Hence, relaxivity measurements of the MNPs in solution do not completely correlate with intracellular relaxivity.

Macrophages exhibited a decreased uptake of particles with higher Mw PEG (Figure 7), and it is evident that the uptake is connected to the physical properties of the nanoparticles, as PEG coatings have

previously been demonstrated to lower the uptake of MNPs in macrophages cells [42]. In another study, 5000 Da PEG coating was observed to be the most optimal length for minimizing plasma protein absorption on poly(lactic acid) nanoparticles [15]. In our study, nanoparticles coated with the longest PEG (20000 Da) exhibited the lowest uptake in cells.

The low uptake of the particles coated with higher Mw of PEG in macrophages correlates well with the increased in circulatory half-life (Figure 8). The low zeta potential of the particles indicates that the charges on the iron oxide are being screened by the PEG coatings minimizing particle interactions with plasma proteins involved in immune activation, opsonization and attachment of the nanoparticles to the cell membrane [36;43].

MRI of MNPs in mouse tumors revealed a significant contrast with variable Mw PEG (Figure 9). The particles coated with 10000 Da PEG showed significantly higher contrast in the SCCVII tumor after injection of nanoparticles. In the C3H tumor, however, no accumulation of nanoparticles could be observed using 3 T MRI, which could indicate tumor specific differences. However, from qualitative high-field 16.4 T MRI scanning of C3H tumors a higher contrast after injection of MNPs coated with 750, 2000, and 10000 Da PEG was observed (Figure 10). Possibly the two tumor models are different regarding how well the EPR effect will work. We can speculate that the C3H tumor model perhaps has smaller or fewer openings in the endothelia lining of the blood vessels, thereby limiting the access of the nanoparticles out of the blood system into the tumor tissue. Taken together these results therefore support that PEG coated MNP accumulate passively in murine tumors and particularly MNPs coated with 10000 Da PEG create a high contrast, particular in the outer rim of the tumor, while particles in the 750-2000 Da PEG range exhibit a general lower contrast that, however, were more evenly distributed over the tumor volume.

The mechanism for accumulation of particles in tumors is probably due to the EPR effect that is enhanced by small nanoparticles with stable coatings that prevent aggregation, a low net charge, and a prolonged circulatory half-life. Through a comprehensive empirical approach we show that these requirements were best achieved by coating MNPs with 10000 Da PEG, which led to an accumulation of the particles in the tumor with an up to 60% increased contrast compared to saline injection.

References:

1. **Harisinghani, M.G.;Barentsz, J.;Hahn, P.F.;Deserno, W.M.;Tabatabaei, S.;van de Kaa, C.H., et al. Noninvasive Detection of Clinically Occult Lymph-Node Metastases in Prostate Cancer.** ***N Engl J Med*** **2003;348(25):2491-99.**
2. **Hyon Bin, N.;In Chan, S.; Taeghwan, H. Inorganic Nanoparticles for MRI Contrast Agents.** ***Advanced Materials*** **2009;21(21):2133-48.**
3. **Larsen, E.K.U.;Nielsen, T.;Wittenborn, T.;Birkedal, H.;Vorup-Jensen, T.;Jakobsen, M.H., et al. Size-Dependent Accumulation of PEGylated Silane-Coated Magnetic Iron Oxide Nanoparticles in Murine Tumors.** ***ACS Nano*** **2009;3(7):1947-51.**
4. **Butterworth, M.D.;Illum, L.; Davis, S.S. Preparation of ultrafine silica- and PEG-coated magnetite particles.** ***Colloids and Surfaces A: Physicochemical and Engineering Aspects*** **2001;179(1):93-102.**
5. **Laurent, S.;Nicotra, C.;Y.Gossuin;Roch, A.;Ouakssim, A.;Elst, L.V., et al. Influence of the length of the coating molecules on the nuclear magnetic relaxivity of superparamagnetic colloids.** ***physica status solidi (c)*** **2004;1(12):3644-50.**
6. **Fee, C.J. Size comparison between proteins PEGylated with branched and linear poly(ethylene glycol) molecules.** ***Biotechnology and Bioengineering*** **2007;98(4):725-31.**
7. **LaConte, L.E.W.;Nitin, N.;Zurkiya, O.;Caruntu, D.;O'Connor, C.J.;Hu, X., et al. Coating thickness of magnetic iron oxide nanoparticles affects R2 relaxivity.** ***Journal of Magnetic Resonance Imaging*** **2007;26(6):1634-41.**
8. **Roberts, M.J.;Bentley, M.D.; Harris, J.M. Chemistry for peptide and protein PEGylation.** ***Advanced Drug Delivery Reviews*** **2002;54(4):459-76.**
9. **van Vlerken, L.;Vyas, T.; Amiji, M. Poly(ethylene glycol)-modified Nanocarriers for Tumor-targeted and Intracellular Delivery.** ***Pharmaceutical Research*** **2007;24(8):1405-14.**
10. **Harris, J.M.; Chess, R.B. Effect of pegylation on pharmaceuticals.** ***Nat Rev Drug Discov*** **2003;2(3):214-21.**
11. **Tiefenauer, L.X.;Tschirky, A.;Kuhne, G.; Andres, R.Y. In vivo evaluation of magnetite nanoparticles for use as a tumor contrast agent in MRI.** ***Magnetic Resonance Imaging*** **1996;14(4):391-402.**
12. **Moghimi, S.M.;Hunter, A.C.; Murray, J.C. Long-Circulating and Target-Specific Nanoparticles: Theory to Practice.** ***Pharmacol Rev*** **2001;53(2):283-318.**
13. **Carroll, M.C. The complement system in regulation of adaptive immunity.** ***Nature Immunology*** **2004;5(10):981-86.**
14. **Allen, T.M. The use of glycolipids and hydrophilic polymers in avoiding rapid uptake of liposomes by the mononuclear phagocyte system.** ***Advanced Drug Delivery Reviews*** **1994;13(3):285-309.**
15. **Gref, R.;Lück, M.;Quellec, P.;Marchand, M.;Dellacherie, E.;Harnisch, S., et al. `Stealth' corona-core nanoparticles surface modified by polyethylene glycol (PEG): influences of the corona (PEG chain length and surface density) and of the core composition on phagocytic uptake and plasma protein adsorption.** ***Colloids and Surfaces B: Biointerfaces*** **2000;18(3-4):301-13.**
16. **Bremer, C.;Allkemper, T.;Baermig, J.; Reimer, P. RES-specific imaging of the liver and spleen with iron oxide particles designed for blood pool MR-angiography.** ***J Magn Reson Imaging*** **1999;10(3):461-67.**
17. **Jain, T.K.;Reddy, M.K.;Morales, M.A.;Leslie-Pelecky, D.L.; Labhasetwar, V. Biodistribution, Clearance, and Biocompatibility of Iron Oxide Magnetic Nanoparticles in Rats.** ***Mol. Pharmaceutics*** **2008;5(2):316-27.**
18. **Weissleder, R.;Stark, D.D.;Engelstad, B.L.;Bacon, B.R.;Compton, C.C.;White, D.L., et al. Superparamagnetic iron oxide: pharmacokinetics and toxicity. 1989;152(1):167-73.**
19. **Moghimi, S.M. Exploiting bone marrow microvascular structure for drug delivery and future therapies.** ***Advanced Drug Delivery Reviews*** **1995;17(1):61-73.**
20. **Soo Choi, H.;Liu, W.;Misra, P.;Tanaka, E.;Zimmer, J.P.;Itty Ipe, B., et al. Renal clearance of quantum dots.** ***Nat Biotech*** **2007;25(10):1165-70.**
21. **Banerjee, T.;Mitra, S.;Kumar Singh, A.;Kumar Sharma, R.; Maitra, A. Preparation, characterization and biodistribution of ultrafine chitosan nanoparticles.** ***International Journal of Pharmaceutics*** **2002;243(1-2):93-105.**
22. **Fee, C.J.; Van Alstine, J.M. Prediction of the Viscosity Radius and the Size Exclusion Chromatography Behavior of PEGylated Proteins.** ***Bioconjugate Chemistry*** **2004;15(6):1304-13.**
23. **Sperling, R.A.;Liedl, T.;Duhr, S.;Kudera, S.;Zanella, M.;Lin, C.A.J., et al. Size Determination of (Bio)conjugated Water-Soluble Colloidal Nanoparticles: A Compari son of Different Techniques.** ***The Journal of Physical Chemistry C*** **2007;111(31):11552-59.**
24. **Gref, R.;Minamitake, Y.;Peracchia, M.T.;Trubetskoy, V.;Torchilin, V.; Langer, R. Biodegradable Long-Circulating Polymeric Nanospheres.** ***Science*** **1994;263(5153):1600-03.**

25. Fang, C.;Shi, B.;Pei, Y.-Y.;Hong, M.-H.;Wu, J.; Chen, H.-Z. In vivo tumor targeting of tumor necrosis factor-[alpha]-loaded stealth nanoparticles: Effect of MePEG molecular weight and particle size. *European Journal of Pharmaceutical Sciences* 2006;27(1):27-36.
26. Matsumura, Y.; Maeda, H. A New Concept for Macromolecular Therapeutics in Cancer Chemotherapy: Mechanism of Tumoritropic Accumulation of Proteins and the Antitumor Agent Smancs. *Cancer Res* 1986;46:6387-92.
27. Vaupel, P. Tumor microenvironmental physiology and its implications for radiation oncology. *Semin Radiat Oncol* 2004;14(3):198-206.
28. Moore, A.;Marecos, E.;Bogdanov, A., Jr.; Weissleder, R. Tumoral Distribution of Long-circulating Dextran-coated Iron Oxide Nanoparticles in a Rodent Model. *Radiology* 2000;214(2):568-74.
29. Brigger, I.;Dubernet, C.; Couvreur, P. Nanoparticles in cancer therapy and diagnosis. *Advanced Drug Delivery Reviews* 2002;54(5):631-51.
30. DePalma, R.;Peeters, S.;VanBael, M.J.;VandenRul, H.;Bonroy, K.;Laureyn, W., et al. Silane Ligand Exchange to Make Hydrophobic Superparamagnetic Nanoparticles Water-Dispersible. *Chem. Mater.* 2007;19(7):1821-31.
31. Zhu, X.Y.;Jun, Y.;Staarup, D.R.;Major, R.C.;Danielson, S.;Boiadjiev, V., et al. Grafting of High-Density Poly(Ethylene Glycol) Monolayers on Si(111). *Langmuir* 2001;17(25):7798-803.
32. Frydman, A.;Castner, D.G.;Schmal, M.; Campbell, C.T. A Method for Accurate Quantitative XPS Analysis of Multimetallic or Multiphase Catalysts on Support Particles. *Journal of Catalysis* 1995;157(1):133-44.
33. Singh, G.;Pillai, S.;Arpanaei, A.; Kingshott, P. Highly Ordered Mixed Protein Patterns Over Large Areas from Self-Assembly of Binary Colloids. *Advanced Materials* 2011;23(13):1519-23.
34. Hardman, R. A Toxicologic Review of Quantum Dots: Toxicity Depends on Physicochemical and Environmental Factors. *Environ Health Perspect* 2006;114(2).
35. MailaÌˆnder, V.; Landfester, K. Interaction of Nanoparticles with Cells. *Biomacromolecules* 2009;10(9):2379-400.
36. Roser, M.;Fischer, D.; Kissel, T. Surface-modified biodegradable albumin nano- and microspheres. II: effect of surface charges on in vitro phagocytosis and biodistribution in rats. *European Journal of Pharmaceutics and Biopharmaceutics* 1998;46(3):255-63.
37. Rowe, M.D.;Chang, C.-C.;Thamm, D.H.;Kraft, S.L.;Harmon, J.F.;Vogt, A.P., et al. Tuning the Magnetic Resonance Imaging Properties of Positive Contrast Agent Nanoparticles by Surface Modification with RAFT Polymers. *Langmuir* 2009;25(16):9487-99.
38. Duan, H.;Kuang, M.;Wang, X.;Wang, Y.A.;Mao, H.; Nie, S. Reexamining the Effects of Particle Size and Surface Chemistry on the Magnetic Properties of Iron Oxide Nanocrystals: New Insights into Spin Disorder and Proton Relaxivity. *The Journal of Physical Chemistry C* 2008;112(22):8127-31.
39. Yigit, M.V.;Mazumdar, D.; Lu, Y. MRI Detection of Thrombin with Aptamer Functionalized Superparamagnetic Iron Oxide Nanoparticles. *Bioconjugate Chem.* 2008;19(2):412-17.
40. Larsen, B.A.; et al. Controlled aggregation of superparamagnetic iron oxide nanoparticles for the development of molecular magnetic resonance imaging probes. *Nanotechnology* 2008;19(26):265102.
41. Bulte, J.W.M.;Douglas, T.;Witwer, B.;Zhang, S.-C.;Strable, E.;Lewis, B.K., et al. Magnetodendrimers allow endosomal magnetic labeling and in vivo tracking of stem cells. *Nat Biotech* 2001;19(12):1141-47.
42. Zhang, Y.;Kohler, N.; Zhang, M. Surface modification of superparamagnetic magnetite nanoparticles and their intracellular uptake. *Biomaterials* 2002;23(7):1553-61.
43. Owens Iii, D.E.; Peppas, N.A. Opsonization, biodistribution, and pharmacokinetics of polymeric nanoparticles. *International Journal of Pharmaceutics* 2006;307(1):93-102.